# Assignment 1: Algorithms Galore!

Computational Statistics
Instructor: Luiz Max de Carvalho

November 20, 2021

**Hand-in date: 22/11/2021.**

## General guidance

- State and prove all non-trivial mathematical results necessary to substantiate your arguments;
- Do not forget to add appropriate scholarly references *at the end* of the document;
- Mathematical expressions also receive punctuation;
- Please hand in a single PDF file as your final main document.

  Code appendices are welcome, *in addition* to the main PDF document.

# Background

By now we have seen quite a few methods for computing integrals *via* Monte Carlo. Each method has its own advantages and drawbacks. It is important that we understand these properties in order to apply the methods effectively. In this assignment we will continue studying the problem of computing the average distance between two points on a disk, this time from the perspective of method comparison. That is to say that in this assignment you will experience the microcosm of comparing several methods for solving a problem for which we happen to know the right answer in closed-form.

Recall that we want to compute

$$\begin{aligned} I &= \frac{1}{\pi^2 R^4} \int_0^R \int_0^R \int_0^{2\pi} \int_0^{2\pi} \sqrt{r_1^2 + r_2^2 - 2r_1 r_2 \cos\phi(\theta_1, \theta_2)} r_1 r_2 \, d\theta_1 \, d\theta_2 \, dr_1 \, dr_2, \\ &= \frac{2^7}{45\pi} R, \end{aligned}$$

where $\phi(\theta_1, \theta_2)$ is the central angle between $r_1$ and $r_2$.

Here we will do something a bit risky: we will compare a few methods to compute $I$ using a bunch of different methods without knowing in advance which will work best or if there are going to be any differences at all. Welcome to Science!

# Methods

Here we will list a selection of methods that will be randomly assigned to each student, along with some questions that need to be answered for that particular method.

- **Rejection sampling**
  - Justify your choice of proposal distribution and show that it conforms to the necessary conditions for the algorithm to work; in particular, try to find a proposal that gives the highest acceptance probability.
- **Importance sampling**
  - Justify your choice of proposal based on the variance of the resulting estimator.
- **Gibbs sampling**
  - Write your full conditionals out and show that they adhere to the Hammersley-Clifford condition.
- **Metropolis-Hastings**
  - Justify your choice of proposal; test different ones if you need to.
- **Static Hamiltonian Monte Carlo**
  - Comment on the choice of step size ($\varepsilon$) and integration time ($\tau$).

# Questions

1. You have been (randomly) assigned a method from the previous section. Represent $I$ as $\int_{\mathcal{X}} \phi(x)\pi(x)\,dx$ and justify your choice of $\phi$, $\pi$ and $\mathcal{X}$. Recall that these choices are arbitrary up to a point, but they might lead to wildly different empirical performances **and** theoretical properties for estimators of $I$. **Justify** your choices in light of the method you have been given to work with. Choose wisely and be rigorous in your justifications.

2. Again, starting from the eventual samples you will obtain with your method, construct a non-empty[1] family of estimators of $I$ and discuss whether it is (strongly) consistent and whether a central limit theorem can be established.

3. Detail a suite of diagnostics that might be employed in your application to detect convergence or performance problems. Extra points for those who design algorithms that exploit the structure of this particular integration problem.

4. For each $R \in \{0.01, 0.1, 1, 10, 100, 1000, 10000\}$, perform $M = 500$ runs from your simulation method and compute: (i) variance (ii) bias (iii) standard deviation of the mean (MCSE).

5. Can you identify one key quantity missing from the previous item? *Hint:* it bears relevance to the real world application of any computational method.

**Warning:** the questions in this assignment might seem deceptively simple; do not be fooled. I expect a lot of effort from you in making your method work the best it can. This entails loads of failed derivations and experiments, which you are encouraged to report in order to document the discovery process. Also, feel free to include answers to questions that have not been asked, if you feel they are relevant. Make loads of figures and tables and let your scientific imagination run wild! Good luck![2]

# Distance between Points: a Very Personal Application [1, 2]

Let us begin restating the problem which we are interested in solving. For that, suppose $X_1, X_2$ come from a uniform distribution $\pi \sim U_{C_R}$, where $C_R$ is a disk of radius $R$ centered at the origin of $\mathbb{R}^2$. Our goal is to calculate the expectation of the Euclidean distance between i.i.d. samples of $X_1$, $X_2$, $\mathbb{E}\|X_1 - X_2\|_2 \equiv \mathbb{E}\|X_1 - X_2\|$. As we have seen in Assignment 0, this expectation is fully given by the integral in $\mathbb{R}^4$ given through

$$I = \frac{1}{\pi^2 R^4} \int_0^R \int_0^R \int_0^{2\pi} \int_0^{2\pi} \sqrt{r_1^2 + r_2^2 - 2r_1 r_2 \cos\phi(\theta_1, \theta_2)}\, r_1 r_2 \, d\theta_1 \, d\theta_2 \, dr_1 \, dr_2, \tag{1}$$

[1] This is a joke. It means you should come up with at least one estimator. But you might, and are even encouraged to, entertain more than one estimator.

[2] I decided to answer these five questions within the text, so to make reading flow smoother. However, to facilitate grader's life easier, I added, at the title of each section, the question numbers it is supposed to answer throughout its text.

which, through the Crofton's Formula for Mean Values, was there shown to be $I = \frac{128\pi}{45}$.

Even though we could solve this problem in closed form (or, perhaps, because we could solve this problem in closed form), we are still interested in applying Monte Carlo techniques to it. Nonetheless, we have many choices of estimators for the integral $I$. Probably the most obvious one comes from seeing the integral $I$ as

$$\begin{aligned} I &= \frac{4\pi^2 R^2}{\pi^2 R^4} \int_{\mathbb{R}^4} \sqrt{r_1^2 + r_2^2 - 2r_1 r_2 \cos\phi(\theta_1, \theta_2)} r_1 r_2 \times \pi_1(\mathbf{x})\, d\mathbf{x} \\ &= \int_{\mathbb{R}^4} f(\mathbf{x}) \pi_1(\mathbf{x})\, d\mathbf{x}, \end{aligned} \tag{2}$$

where $\pi_1(\mathbf{x})$ is the density of the uniform distribution on $D = [0, R] \times [0, R] \times [0, 2\pi] \times [0, 2\pi] \subseteq \mathbb{R}^4$, given by $\pi_1(\mathbf{x}) = \frac{1}{4\pi^2 R^2} \times I_D$, where $I_D$ be the identity function taking values of 1 exactly at the disk $D$ and zero elsewhere and

$$\begin{aligned} f(\mathbf{x}) &= \frac{4\pi^2 R^2}{\pi^2 R^4} \sqrt{r_1^2 + r_2^2 - 2r_1 r_2 \cos\phi(\theta_1, \theta_2)} r_1 r_2 \\ &= \frac{4}{R^2} \sqrt{r_1^2 + r_2^2 - 2r_1 r_2 \cos\phi(\theta_1, \theta_2)} r_1 r_2. \end{aligned}$$

Such way of restating the problem suggests a Monte Carlo estimator for equation (2), given through

$$\hat{I}_1 = \frac{1}{N} \sum_{i=1}^{N} f(\mathbf{x}_i),$$

where $\mathbf{x}_i$ are sampled from $\pi_1(\mathbf{x})$. Notice that the expectation of this estimator turns out to be

$$\begin{aligned} \mathbb{E}_{\pi_1(\mathbf{x})} \hat{I}_1 &= \frac{1}{N} \sum_{i=1}^{N} \mathbb{E}_{\pi_1(\mathbf{x})} f(\mathbf{x}_i) \\ &= \mathbb{E}_{\pi_1(\mathbf{x})} f(\mathbf{x}_i) \\ &= \int_{\mathbb{R}^4} f(\mathbf{x}) \pi_1(\mathbf{x})\, d\mathbf{x}, \end{aligned}$$

that is, exactly equation (2). In particular, if we can show $\hat{I}_1$ strongly consistent (i.e. $\hat{I}_1 \xrightarrow{\text{a.s.}} \mathbb{E}_{\pi_1(\mathbf{x})} \hat{I}_1$), then it follows that $\hat{I}_1 \xrightarrow{\text{a.s.}} I$. Strong consistency, nonetheless, follows by Kolomogrov's Strong Law of Large Numbers, which says that, provided $\mathbf{y}_i$ independent and identically distributed from some random variable $Y$ for all $i \in \mathbb{Z}^+$, if $Y$ is integrable, then strong, indeed, $\overline{\mathbf{y}_i} \xrightarrow{\text{a.s.}} \mathbb{E}Y$. However, integrability of $Y = f(X)$ given $X \sim U_{C_R}$ follows from noticing that the distribution is limited by

$$\frac{4\sqrt{R^2 + R^2 - 2R\cos\phi(\theta_1, \theta_2)} R^2}{R^2} \leq 4\sqrt{2R^2 + 2R}$$

in all $D$ for fixed $R$, and zero elsewhere. On the other hand, given that $D$ is a Cartesian product of compact intervals, is itself a compact set in $\mathbb{R}^4$ by Tychonoff's theorem [Singer and Thorpe (2012)]. In fact, a similar comparison argument can be used to show that, given $d\pi_1(\mathbf{x}) = 1/4\pi^2 R^2\, d\mathbf{x}$ being non-zero

on a compact set only and $f^3(\mathbf{x}) \leq \frac{4\sqrt{2}R^3}{R^2}$ there, we can guarantee some sort of Monte Carlo version of a Central Limit Theorem for the estimator $\hat{I}_1$, which we shall formalize later, when sampling using Hamiltonian (Hybrid) Monte Carlo (HMC) [Gamerman and Lopes (2006)]. For now, though, it is enough to know that $\mathrm{Var}_{\pi_1} f(\mathbf{x})$ is well-defined thanks to another comparison argument, which restricts the second order absolute momentum of $f$.

For a second estimator, we may again see the integral as the original problem, that is, $I = \mathbb{E}\|X_1 - X_2\|$, being $X_1, X_2 \sim U_{C_R}$, so that, letting $I_{C_R}$ be the identity function taking values of 1 exactly at the disk $C_R$ and zero elsewhere

$$\begin{aligned} I &= \int_{\mathbb{R}^2}\int_{\mathbb{R}^2} \|x_1 - x_2\| \left(I_{C_R} \times I_{C_R}\right) dx_1\, dx_2 \\ &= \int_{\mathbb{R}^4} f(\mathbf{x}) \cdot \pi_2(\mathbf{x})\, d\mathbf{x}, \end{aligned}$$

where $\pi_2(\mathbf{x}) \equiv \pi_2(x_1, x_2)$ is a joint density in $\mathbb{R}^4$ of $X_1, X_2$, taken independently, and $f : \mathbb{R}^2 \to \mathbb{R}$ a deterministic map. Again, we may simply define another estimator through

$$\hat{I}_2 = \frac{1}{N}\sum_{i=1}^{N} \|x_{1_i} - x_{2_i}\|, \tag{3}$$

where $x_{1_i}$ and $x_{2_i}$ are independent realizations of the distributions $X_1$ and $X_2$. Notice that

$$\begin{aligned} \mathbb{E}_{\pi_2(\mathbf{x})}\hat{I}_2 &= \frac{1}{N}\sum_{i=1}^{N} \mathbb{E}_{\pi_2(\mathbf{x})}\|x_1 - x_2\| \\ &= \mathbb{E}_{\pi_2(\mathbf{x})}\|x_1 - x_2\| \\ &= \int_{\mathbb{R}^4} \|x_1 - x_2\|\, \pi_2(x_1, x_2)\, dx_1\, dx_2. \end{aligned}$$

With this, it is again easy to see the consistency of $\hat{I}_2$ through Kolomogrov's, as it is enough to notice that $0 \leq \|x_1 - x_2\| \leq 2R \times I_{C_R \times C_R}$ for all $N \in \mathbb{Z}^+$ and, by compactness of $C_R \times C_R$ (Tychonoff's theorem), $2R \times I_{C_R \times C_R}$ is integrable, so also must be $f(\mathbf{x})$. Finally, we may again limit $f^3(\mathbf{x}) \leq 8R^3$ which, as mentioned, shall be later used for developing a Central Limit Theorem for $\hat{I}_2$.

We will see that, in terms of the Hamiltonian approach, the second estimator $\hat{I}_2$ is much more complicated to devise. However, it permits us to explore possibilities in HMC sampling for uniform distributions in compact surfaces which are not polytopes, which is pretty much worth the effort. Besides, the connection to sampling in $C_R$ allows us to develop some interesting diagnostic techniques exclusive to $\hat{I}_2$.

# The Hamiltonian Approach to Monte Carlo [3]

We will not here give a full review of the Hamiltonian Monte Carlo approach, but rather refer the reader to [Neal (2011); Betancourt (2018)]. However, there are a few aspects of this technique that will be important to what follows. First,

we will assume the Hamiltonian (function) associated to a target distribution $\pi$ as of form

$$H(\mathbf{x}, \mathbf{p}) = -\log \pi(\mathbf{x}) - \log(q(\mathbf{p}|\mathbf{x})),$$

and the associated canonical (Boltzmann-Maxwell) distribution given by

$$P(\mathbf{x}, \mathbf{p}) = \frac{1}{Z} \exp(-H(\mathbf{x}, \mathbf{p})). \tag{4}$$

It is well-known that (4) is invariant under the chain defined by the HMC, which consists in updating an initial state $\mathbf{x}_{(i-1)}$ and a momentum vector $\mathbf{p}$ sampled from the multivariate normal $N(0, M)$, where $M$ is known as the mass matrix, through Hamilton's equations

$$\dot{x}_j = \frac{\partial H(\mathbf{x}, \mathbf{p})}{\partial p_j} \quad \dot{p}_j = -\frac{\partial H(\mathbf{x}, \mathbf{p})}{\partial x_j} \tag{5}$$

for all components $j$ of the vectors $\mathbf{x}$ and $\mathbf{p}$.

It is not always feasible (or even possible) to analytically solve (5), therefore we should consider some numerical integration techniques as well. Among these procedures, of particular interest is the leapfrog, which, given a time step $\epsilon$ and and an integration time of size $L\epsilon$, follows Algorithm 1.

**Algorithm 1** Leapfrog method

**for** run $= 1, 2, ..., L$ **do**
  $p_j \leftarrow p_j - \frac{\epsilon}{2} \frac{\partial U}{\partial x_j} \|_{x_j}$
  $x_j \leftarrow x_j + \epsilon \frac{p_j}{m_j}$
  $p_j \leftarrow p_j - \frac{\epsilon}{2} \frac{\partial U}{\partial x_j} \|_{x_j}$
**end for**

After a full integration cycle, a new state $(\mathbf{x}', \mathbf{p}')$ is accepted as $(\mathbf{x}_{(i)}, \mathbf{p}_{(i)})$ with probability

$$\alpha = \min(1, \exp(H_0(\mathbf{x}_{(i-1)}, \mathbf{p}) - H(\mathbf{x}', \mathbf{p}')), \tag{6}$$

where $\mathbf{p}$ is the momentum sampled from the multivariate normal; otherwise $\mathbf{x}_{(i)} = \mathbf{x}_{(i-1)}$. As [Betancourt (2018)] points out, the only reason why we even need to consider (6) is because of some error introduced by the discritatization of leapfrog: if the system were to be updated according to continuous solutions of equation (5), then the value $H(\mathbf{x}, \mathbf{p})$ would be constant throughout all time steps, therefore the acceptance probability given by (6) would always be 1. Furthermore, we should also point out that equation (6) only assumes such a simple form because the map induced though the flow of Hamilton's equations (5) preserves the volume in the $\mathbf{x} \times \mathbf{p}$-space, due to a result known as Liouville's Theorem. If that was not to be the case, an extra term from the Jacobian determinant $\| \frac{\partial(\mathbf{x}', \mathbf{p}')}{\partial(\mathbf{x}_{(i-1)}, \mathbf{p})} \|$ would show up, complicating things significantly. On the other hand, the Jacobian would still show up was not for the leapfrog also being volume preserving [Mohasel Afshar et al. (2021)], characteristic which makes it a *sympletic integrator*.

It is fascinating to notice that results such as Liouville's exist much before the publishing of Metropolis' paper, not to mention the development of HMC

itself [Liouville (1838)]. This is because the study of Hamiltonian dynamics, i.e. structures which respect equations (5), is of great interest on its own. It turns out that any enough well-behaved classical physical system consisting of $n$ particles in a $d$-dimensional space is Hamiltonian[3], where $\mathbf{x}$ are coordinates used to represent particles' positions and $\mathbf{p}$ are their generalized momenta. Within this interpretation, the Hamiltonian function $H(\mathbf{x}, \mathbf{p})$ is often associated to the system's total mechanical energy, i.e. the sum of its kinetic and potential energies. Consequently, conservation of the Hamiltonian throughout the integral curves of equation (5) suddenly gains extra weight: it becomes a statement of conservation of energy.

Still in this physical framework, the special case where the coordinates of $\mathbf{x}$ are Cartesian – i.e. orthonormal and translation invariant – has the term $K(\mathbf{x}, \mathbf{p})$, interpreted as the system's kinetic energy, as

$$K(\mathbf{x}, \mathbf{p}) = \frac{1}{2} \sum_j \frac{p_j^2}{m_j} = \frac{1}{2} \mathbf{p}^T M^{-1} \mathbf{p},$$

in which we assume the mass matrix $M$ of diagonal of entries $m_j$, each particles' mass [4]. It is also convenient to assume $U$, here called the potential energy, to depend only on the original coordinates $\mathbf{x}$, assumption which is quite essential for conservation of energy [Taylor (2005)]. Hamilton's equations in this scenario reduce to

$$\dot{x}_j = \frac{p_j}{m_j} \quad \dot{p}_j = -\frac{\partial U(\mathbf{x})}{\partial x_j}, \tag{7}$$

or in vector form,

$$\dot{\mathbf{x}} = \frac{\mathbf{p}}{\mathbf{m}} \quad \dot{\mathbf{p}} = -\nabla U(\mathbf{x}),$$

with $\mathbf{m} = (m_1, ..., m_n)$. The first of these equations is the traditional definition of linear momentum and the second is widely known in literature as Newton's Second Law.

Surprisingly, the connection between HMC and classical system is even stronger when we take the momentum distribution $q(\mathbf{p}|\mathbf{x})$ to be a multivariate normal $(2\pi|M|)^{-d/2} \exp(-\frac{1}{2} \mathbf{p}^T M^{-1} \mathbf{p})$, then giving the Hamiltonian

$$H(\mathbf{x}, \mathbf{p}) = \frac{1}{2} \mathbf{p}^T M^{-1} \mathbf{p} + \frac{n}{2} \log 2\pi|M| + U(\mathbf{x}).$$

Therefore, if we take $U(\mathbf{x}) = \log \pi(\mathbf{x})$ for our target distribution $\pi(\mathbf{x})$, the dynamics of the HMC sampler becomes exactly the one of a classical system described by Newtonian mechanics of equations (7), which describe a particle under the influence of a scalar potential field $U(\mathbf{x})$. We can thus understand the Metropolis-Hastings part of the HMC – i.e. the integration portion of motion – as a simple mathematical realization of some physical system! This point of view will be useful in the next sections when we face problems with compact support, but for now, let us digress a little and consider some convergence results and suitable diagnostics to HMC.

[3] I will not discuss here what it means for a physical system to be enough well-behaved, but rather refer the reader to any advanced text on analytical mechanics such as [Taylor (2005)].

[4] This is often a cause of confusion, even in analytical mechanics. For a system consisting of $n$ particles in a $d$ dimensional space, we have $n \times d$ coordinates for the vectors $\mathbf{x}$ and $\mathbf{p}$, where only $n$ potentially distinct masses $m_j$, that is, $M = \text{diag}(m_1, m_1, ..., m_1, ..., m_2, m_n, ..., m_n)$.

As a Markov method, Hamiltonian chains are very prone to autocorrelate its terms, which can cause severe problems in generating really independent samples. Although this may increase mixing time, the impact in convergence to the stationary canonical distribution should be little, but clearly there is a potential growth in variance. To compute this influence, we let an estimator based on the chain entries $X_{(i)}$ be $t_{(i)} = t(X_{(i)})$ and define, for all lags $k \in \mathbb{N}$, $\gamma_k = Cov_\pi(t_{(i)}, t_{(i+k)})$. Consequently, the variance of $t_{(i)}$ is $\gamma_0 = \mathrm{Var}_\pi t_{(i)}$ and the autocorrelation factors are $\rho_k = \frac{\gamma_k}{\gamma_0}$. We then have the the full chain's average $\bar{t}_N = \frac{1}{N}\sum_{i=1}^{i} t(X_i)$ and the variance of this average estimator becomes $\frac{\tau_N^2}{N} = \mathrm{Var}_\pi(\bar{t}_N)$. It is shown that [Gamerman and Lopes (2006)]

$$\tau_N^2 = \mathrm{Var}_\pi(t_{(i)})\left(1 + 2\sum_{k=1}^{N-1}\frac{N-k}{k}\rho_k\right)$$

and then $\tau_N^2 \to \tau^2$, where

$$\tau^2 = \mathrm{Var}_\pi(t_{(i)})\left(1 + 2\sum_{k=1}^{\infty}\rho_k\right), \tag{8}$$

provided the series converges. Notice that if the sampling is independent,

$$\tau^2 = \mathrm{Var}_\pi(t_{(i)}),$$

so we have a Central Limit Theorem given by

$$\sqrt{n}\frac{\bar{t}_N - \mathbb{E}_\pi(t_{(i)})}{\sqrt{\mathrm{Var}_\pi(t_{(i)})}} \xrightarrow{d} N(0,1). \tag{9}$$

In general, nonetheless, non-zero autocorrelation factors shift the the Central Limit Theory as they modify the variance of $\bar{t}$. We can update its variance by considering what would be the necessary independent sample size, $n_{eff}$, to have asymptotic variance $\mathrm{Var}_\pi(\bar{t}_N) = \frac{\mathrm{Var}_\pi(t_{(i)})}{n_{eff}}$. We thus note

$$n_{eff} = \frac{n}{1 + 2\sum_{k=1}^{\infty}\rho_k}, \tag{10}$$

which allows to rewrite (9) as

$$\sqrt{n_{eff}}\frac{\bar{t}_N - \mathbb{E}_\pi(t_{(i)})}{\sqrt{\mathrm{Var}_\pi(t_{(i)})}} \xrightarrow{d} N(0,1),$$

provided the chain is geometrically ergodic. The requirement for geometric egordicity is far from easy to establish and, although [Livingstone et al. (2019)] gives some guidelines in ensuring it, the process is better done in a case by case scheme.

Estimating $\tau$ is no easy task. First, we must ensure that the series in (8) converges, which is often done by calculating

$$\hat{\rho}_k = \frac{1}{N\hat{\gamma}_0}\sum_{j=1}^{N-k}(t_{(j)} - \bar{t})(t_{(j+k)} - \bar{t}) \tag{11}$$

and testing whether this is smaller than $\frac{1}{k^2}$ for all large enough $k \in \mathbb{N}$. To actually estimate $\tau$, [Gamerman and Lopes (2006)] suggests batching the chain into $k$ groups of $m$ successive values and take the batch averages $\bar{t}_1, ..., \bar{t}_k$. For large enough $k$ and $m$, the batch averages tend to $\mathbb{E}_\pi(t_{(i)})$ and we may estimate $\tau^2$ as

$$\hat{\tau}^2 = \frac{n}{k(k-1)} \sum_{i=1}^{k} (\bar{t}_i - \bar{\bar{t}}), \tag{12}$$

where $\bar{\bar{t}}$ is the average of batch averages, which is just the full chain average. This allows to formulate a new Central Limit result

$$\sqrt{n} \frac{\bar{t} - \mathbb{E}_\pi(t_{(i)})}{\hat{\tau}} \xrightarrow{d} t_{k-1}(0,1), \tag{13}$$

where Student's t-distribution is taken to account for the extra uncertainty introduced by $\hat{\tau}$.

Finally, we can apply the usual Markov Chains Monte Carlo diagnostic techniques to HMC. One that is particular popular is the Gelman and Rubin method [Gelman and Rubin (1992)], that consists in running $m$ chains of length $n$, computing the quantities

$$B = \frac{n}{m-1} \sum_{i=1}^{n} (\bar{t}_i - \bar{\bar{t}}) \quad W = \frac{1}{m(n-1)} \sum_{i=1}^{m} \sum_{j=1}^{n} (t_{(i)}^{(j)} - \bar{t}_{(i)})$$

and the associated ratio

$$\hat{R} = \sqrt{\frac{(1-1/n)W + B/n}{W}},$$

which indicates good convergence when close to 1 (values around $\hat{R} \leq 1.1$ are often taken to be good enough).

Other diagnostic techniques are also recommended for Markov chains: Geweke [Geweke (1991)] suggests comparing the ergodic averages at the beginning and end of the convergence time, which should be approximated by a normal distribution for large values; trace plots are useful not only because they measure convergence, but also because their rate is an indicator of uniform ergocity, when faster than exponential [Gamerman and Lopes (2006)]. When the time comes, we will use all these techniques to assess the qualities of $\hat{I}_1$ and $\hat{I}_2$, together with some other diagnostics based on the geometry of target distributions $\pi$, but, before we can investigate convergence, we must first apply HMC to our estimators.

Let us start with $\hat{I}_1$. We take, to be able to use the physical analogy, $q(\mathbf{p}|\mathbf{x}) = \mathbf{p} \sim N(0, M)$ and $U(\mathbf{x}) = -\log \pi_1(\mathbf{x})$, where

$$\pi_1(\mathbf{x}) = \begin{cases} \frac{1}{4\pi^2 R^2} \text{ if } x \in D \\ 0 \text{ elsewhere.} \end{cases}$$

This implies the potential $U$ to be $\log 4\pi^2 R^2$ and of null derivative inside the distribution's support $D$, that is, $\dot{\mathbf{p}} = 0$. Nevertheless, outside the support, we have $U(\mathbf{x}) \to \infty$, making any possible attempt of applying equations (5) worthless. Unfortunately, the situation is even worse as this kind of divergence

in $U$ will happen whenever the target distribution $\pi$ has a compact support, making estimating $\hat{I}_2$ also out of question! What are we to do now? Can we somehow still use the divergent potential as if $\infty$ was a really large number and hope that the HMC will not sort points there? Is there any other way to tackle this problematic situation of bounded support that might even *improve* the quality of the estimators? We will develop, in what follows, solutions to all of these questions, but to simplify matters as we present these approaches, we will make a detour and investigate an easier version of this scenario, a version that already has physical interest on its own.

## The Compact Support Issue

As it turns out that the problem with boundaries which we identified in the last section only exists because of the discritization introduced while solving Hamilton's equation. Let us consider, for now, the physical system known as the infinite well: a particle of mass $m$ and known momentum $p$ in a 1-dimensional space, of potential energy

$$U(x) = \begin{cases} a & \text{if } 0 \leq x \leq 1 \\ +\infty & \text{elsewhere,} \end{cases}$$

as $a$ is some fixed real number (Figure 1). Astoundingly, this system is well-study in its quantum mechanics counterpart, often quoted as one of the easiest to compute examples of discretization of energy – i.e. restriction of particles to occupy only integer multiples of some ground energy level – that young physicists encounter and the theoretical basis behind the technology known as quantum dot, often found within contemporary television screens [Harris (2016); Beck (2012)]. Through the HMC-physical correspondence, it is not hard to see that the infinite well can be used to sample from a uniform distribution $U_{[0,1]}$, where here, we retrieve the potential energy

$$U(x) = \begin{cases} -\log(1) = 0 & \text{if } 0 \leq x \leq 1 \\ -\log(0) = +\infty & \text{elsewhere.} \end{cases}$$

We are again faced with the problem of compact support: outside the $[0, 1]$ range, the potential energy diverges, so it does not even make sense to consider the derivative $\frac{\partial U}{\partial x}$ at these places. How are we supposed to proceed?

The most natural solution is to exploit the lack of definition of the function $U$ and simply propose some deterministic value for $\frac{\partial U}{\partial x}$. Because outside $[0, 1]$ the potential energy is infinite, whenever the sampled particle falls within the exterior region, the Hamiltonian diverges to infinity and the acceptance proposal $\alpha$ becomes

$$\alpha = \min(1, \exp(H_0(x_0, p_0) - H(x, p)) \to \min(1, \exp(-\infty)) = 0,$$

implying that, necessarily, the particles outside the target's support will be discarded. Good care in the choice of $\frac{\partial U}{\partial x}$ is still necessary. If any chosen value makes a particle whose leapfrog trajectory lead out of $[0, 1]$ be brought back to the interval, then we might induct some deviations from the "Hamiltoniaty" of

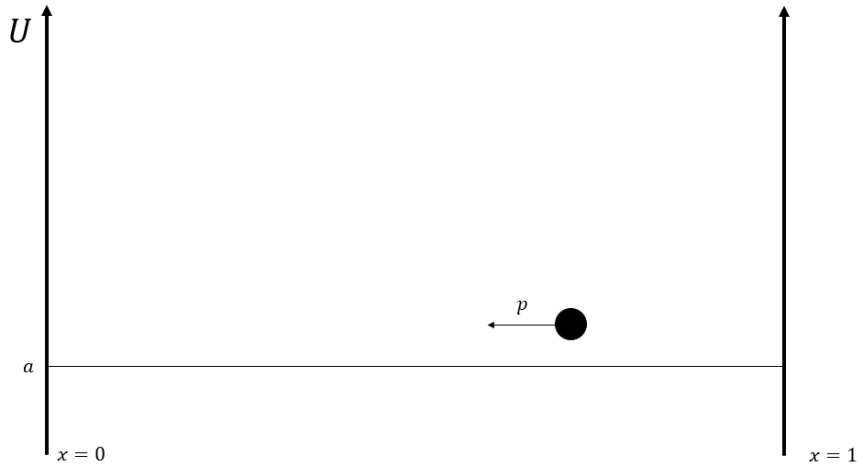


Figure 1: Depiction of a particle of linear momentum $p$ trapped in an infinite well potential energy in the interval $[0, 1]$.

the process, therefore not necessarily keeping the stationary status of the canonical distribution. We then want a particle that enters the "forbidden region" to stay there, allowing for the Metropolis-Hastings ratio step $\alpha$ to determine its deletion. One possibility is to keep $\frac{\partial U}{\partial x} = 0$, letting inertia drive the particle away from the borders of $[0, 1]$; other is to simply halt the particle as soon as we notice that it has entered the forbidden region – doing so completely kills the dynamics of the system, but it hardly matters, as we will discard the particle anyways.

There is nothing wrong with the solution we have just presented: it fully respects the Hamiltonian dynamics for the accepted particles, the leapfrog method is still sympletic, the process is fully reversible, and we can still expect, again without formal proof, ergocity of the chain. However, when discarding so many points, the acceptance drops significantly: in our simulations, we were able to obtain maximum acceptance rates of good convergence chains of only 15%. This is because, for this kind of compact support constant density problem, in which we simply ignore points in the forbidden region, the HMC reduces to a simple random walk Metropolis-Hastings with proposal distribution given by a Gaussian. This Markov chain seems to indicate convergence towards the target $U_{[0,1]}$, but it seems prohibitively slow and, even worse, it betrays the whole idea behind HMC in using the geometry of the target to speed up sampling.

Nonetheless, this issue is fixable, in fact, we can modify HMC to keep the acceptance rate virtually at 100%. To understand this new technique, let us start considering what goes differently between the physical system of a particle in an infinite well and the classical version of the HMC when we have compact supports. It is easy to see that, for a Hamiltonian system, the particle never really leaves the $[0, 1]$ interval. Whenever the particle reaches one of the boundary

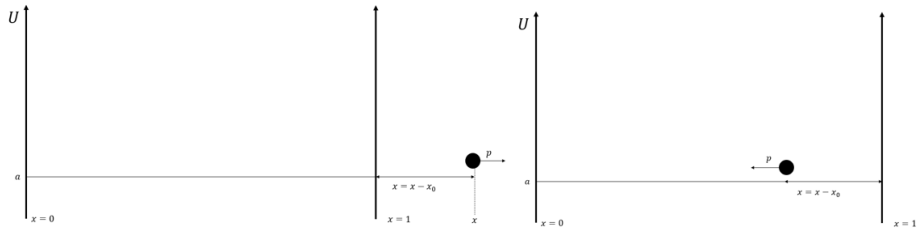


Figure 2: Image showing the conceptual idea behind Reflective Hamiltonian Monte Carlo for target $U_{[0,1]}$, in which a particle with momentum $p$ in the positive direction crosses the border $x_0 = 1$ and travels $x - x_0$ in the forbidden region (left side). For the reflexive step, the particle has its momentum negated to $-p$ and then is positioned at $x_0 - (x - x_0)$ (right side).

points, say $x_0 = 1$, its potential energy gradient becomes

$$\frac{\partial U}{\partial x} = -\infty, \tag{14}$$

Substituting (14) in Hamilton's equation yields

$$\dot{p} = -\infty,$$

indicating that, suddenly, there is an infinite force that makes the particle switches its direction of motion which, initially going to larger values of $x$, now has is reflected back towards lower ones. However, preservation of the Hamiltonian requires that new reflected momentum $p'$ which the particle acquires *after* reaching $x_0 = 1$ to be of same magnitude as the one prior to the collision, that is, $p' = -p$. We call this type of movement of *reflection*, exactly because it describes, in classical terms, what happens when a photon reaches normally the surface of a mirror. The same process takes place when the particle reaches the $x_0 = 0$ boundary, only difference being that the collision flips the initially negative momentum to a same magnitude positive one.

If, however, reflection is what goes down in the classical counterpart of a HMC sampler for $U_{[0,1]}$, why we do not see it happens when using leapfrog? The issue appears exactly because of the discretization of motion. In leapfrog (as well as in any integration technique), the gradient $\frac{\partial U}{\partial x}$ is computed only at discrete time-steps multiples of $\epsilon$. Therefore, if the particle happens to cross out of the allowed region at a non-multiple value of $\epsilon$, leapfrog has no way of knowing that this "forbidden motion" happened, only "seeing" the particle again when it is already at a point it was not supposed to be found, never having the chance to reflect its motion just as the continuous integration of Hamilton's equation would suggest. Consequently, it is not that the leapfrog is wrong, by any means, it is just that it fails to capture the continuity necessary for the dynamics to be correct described.

There are a few workaround the reflection problem. One could, in principle, significantly decrease the values of $\epsilon$ and $m$, make the momentum $p$ switch signs at 0 and 1, and increase the value of $L$ so to allow the sampler, even with such small step values $\epsilon$, to explore the full support of the target. Such measures

do increase the acceptance rate, however, not only they will slow mixing down, often requiring thinning techniques to allow for good independence sampling, but we would always still have, no matter how small the value of $\epsilon > 0$, a non-zero probability that the particle will cross out the allowed region unreflected, so never truly solving the problem.

We can, still, consider changing leapfrog to allow room for reflections. In this new method, which is known in literature as Reflective Hamiltonian Monte Carlo (RHMC) [Afshar et al. (2015); Chevallier et al. (2018); Pakman and Paninski (2014); Ruján (1997)], whenever a particle is detected outside the allowed region by the integration algorithm, we simply take, whatever was its motion in the forbidden region and exactly reflect it across the boundary. To have a conceptual idea of how this process takes place, refer to Figure 2. Suppose that, in a step interval of duration $\epsilon$, the particle initially at[5] $(x_{(i-1)}, p)$ flies away from the constraint $x_0 = 1$ and walks a total of $x - x_0$ in the forbidden region, during an interval of time $\Delta = (x - x_0)\frac{m}{p}$. Then, to reflect this motion back to the allowed interval, we simply make the updated position with reflected momentum $p' = -p$ as $x_{(i)} = x_0 + \Delta \times \frac{p'}{m} = x_0 - (x - x_0)$, that is, we perfectly simulate as if the leapfrog was able to recognize the boundary and performed the reflection on its own. When, on the other hand, the particle crosses towards value smaller than $x_0 = 0$, the reflected proposal becomes $x_{(i)} = x_0 + (x_0 - x)$. A formalization of RHMC for the case of constant coordinate constraints (where all constraints are of form $x_i \leq x_0$ or $x_i \geq x_0$ for some coordinate $x_i$) is described in Algorithm 2.

Extra care is still necessary. It could be that RHMC spoils some of the nice properties of the original method. In particular, we must still verify that the new technique maintains the canonical distribution invariant and that the integration method still preserves volumes. Fortunately, the first of this assertion is clearly true, as RHMC preserves the correct Hamiltonian again, which leaves the canonical distribution invariant, as shown in [Chevallier et al. (2018)], and [Afshar et al. (2015)] gives a proof of the second for general affine constraints in the coordinates $\mathbf{x}$. Ergocity is still an issue and, as far as I can tell, there are no entries in literature dedicated to showing it as a result, not alone its geometric extension. However, for our particular case, there seems not to exist any periodicity independent of momentum that might affect irreducibility of the chain and the empirical convergence diagnostics for our problem, which we will discuss shortly, seem to suggest that we may assume, at least, the weaker version of a Ergodic Theorem.

Figure[6] 3 shows a histogram created from 500 RHMC chains of 1000 points each for the target distribution $\pi \sim U_{[0,1]}$ for $M = 1$. In performing the analysis, we are free to choose fairly large $\epsilon$ values, since reflection is supposed to keep acceptance rate high (in fact, we measured acceptance rate of 100% for all our experiments), but not too large, as this would imply many reflections, which gives many while loops, increasing the computational cost. It seems reasonable

[5]There is an unfortunate confusion in notation here: before $x_{(i-1)}$ and $(x_{(i)})$ were used, respectively, to indicate the the system's configuration at the beginning and end of *a full integration loop of L steps*, but in the discussion here, it represents the beginning and end of a single *integration step*. Although this is a awful abuse of notation, it is not only common in literature, but avoids the use of too many incomprehensible prime symbols.

[6]All code is available in a Jupyter notebook in `https://github.com/HLovisiEnnes/Practice_problems/tree/main/Assignment_1-Computational%20Statistics`.

**Algorithm 2** Reflective Hamiltonian Monte Carlo

Choose $\mathbf{x}_{(0)}$ in the support of $\pi$
**for** $i = 1, 2, ...$ **do**
  $\mathbf{p} \leftarrow N(0, M)$
  $H_0 \leftarrow T(\mathbf{x}_{(i-1)}, \mathbf{p}) + U(\mathbf{x}_{(i-1)}, \mathbf{p})$
  **for** run $= 1, 2, ..., L$ **do**
    $p_j \leftarrow p_j - \frac{\epsilon}{2} \frac{\partial U}{\partial x_j} \|_{x_j}$
    $x_j \leftarrow x_j + \epsilon \frac{p_j}{m_j}$
    **while** $x_j < l_j$ or $x_j > u_j$ for some coordinate $j$ of $\mathbf{x}$ **do**:
      $p_j = -p_j$
      **if** $x_j < l_j$ **then**
        $x_j \leftarrow l_j + (l_j - x_j)$
      **else if** $x_j > u_j$ **then**
        $x_j \leftarrow u_j - (x_j - u_j)$
      **end if**
      $p_j \leftarrow p_j - \frac{\epsilon}{2} \frac{\partial U}{\partial x_j} \|_{x_j}$
    **end while**
  **end for**
  $H \leftarrow T(\mathbf{x}, \mathbf{p}) + U(\mathbf{x}, \mathbf{p})$
  **if** sample from $U_{[0,1} \leq \exp H_0 - H$ **then**
    $\mathbf{x}_{(i)} \leftarrow \mathbf{x}$
  **else**
    $\mathbf{x}_{(i)} = \mathbf{x}_{(i-1)}$
  **end if**
**end for**

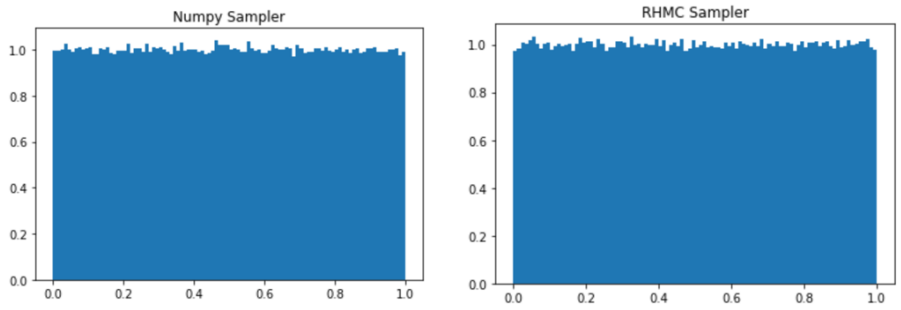


Figure 3: Histograms for the target $\pi$ for $5 \times 10^5$ points through numpy implemented sampler (left side) and Reflective Hamiltonian Monte Carlo sampler (right side).

to keep at average 1 reflection per full iteration time, $L \times \epsilon$, meaning that, if we want to keep $L = 100$ just as suggested by [Neal (2011)], we may use that the average magnitude of momentum given $M = 1$ is $\sqrt{\frac{2}{\pi}}$, and so keep $\epsilon \approx \frac{1}{100} \times \sqrt{\frac{2}{\pi}} = 0.013 \approx 0.01$. We also have added a warm-up period of 30 iterations to avoid early on transient behavior. By the way, to choose the initial value of $x_{(0)}$, we simply sorted from a standard normal distribution centered at 0.5 until we got a value for $x_{(0)}$ inside the $[0, 1]$ interval – nothing more than an easy rejection sampling. The visual diagnostics suggests pretty descent convergence of the RHMC estimator compared to the built-in uniform generator of numpy (left side of Figure 3), although the computation period was at least two orders of magnitude bigger for the RHMC: this should come as no surprise since Markov based models are already much slower than independent sampling techniques, which is even worsen given the while loops in the implementation of Algorithm 2.

# Back to the Disk [4]

Figure 4 shows trace plots for 30 iterations warmed-up traditional HMC and RHMC for estimator $\hat{I}_1$ with $R = 1$, where the target distribution $\pi_1$ is uniform in the set $D$, with $D$ constrained by

$$\begin{aligned} 0 \leq r_1 \leq R \\ 0 \leq r_2 \leq R \\ 0 \leq \theta_1 \leq 2\pi \\ 0 \leq \theta_2 \leq 2\pi. \end{aligned}$$

For both samplers, we kept all $m$ equal 1, $L = 100$ and chose $\mathbf{x}_0$ through a rejection sampling using an independent multidimensional normal distribution in $D$. It is clear that convergence is much better for the reflexive method, even when $\epsilon$ was fine-tuned at $\epsilon = 0.005$ in the traditional HMC. In fact, since acceptance rate is kept at 1 for the RHMC, it makes little difference what $\epsilon$ we

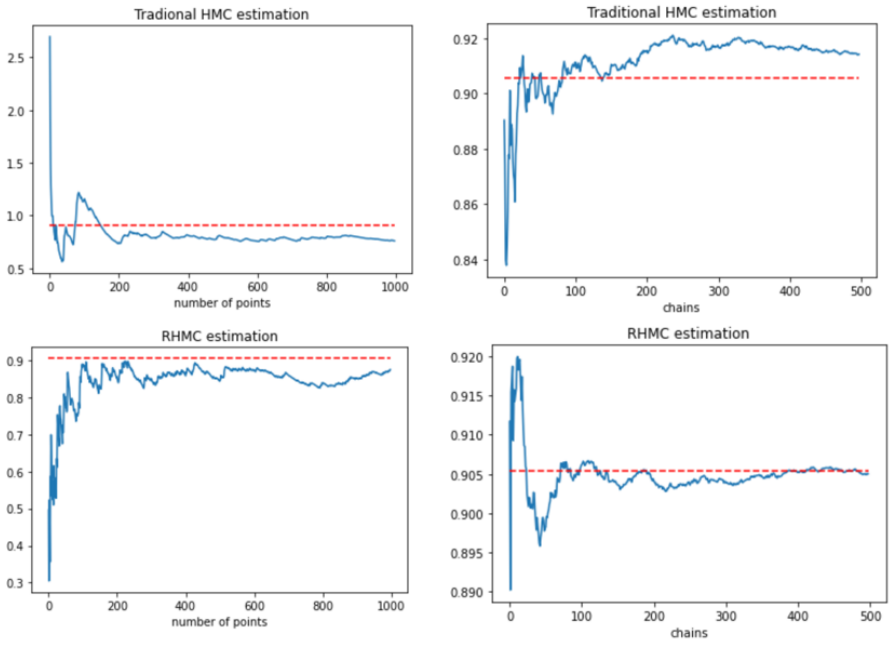


Figure 4: Trace plots for estimations of $\hat{I}_1$ using traditional HMC (up) and RHMC (bottom), with varying number of sample points (left) and number of chains (right), with each chain allowing for an average estimation of 1000 points. Red dashed line indicates the theoretical expected value of $\frac{128}{45\pi}$ given this choice of $R = 1$. For both estimators, we set all $m$ equal 1, $L = 100$, chose $\mathbf{x}_0$ through a rejection sampling using an independent multidimensional normal distribution in $D$, and used $\epsilon = 0.005$ for the traditional HMC, found through fine-tuning, and 0.01 for the HMC.

choose for this approach, with very large $\epsilon$ only to be avoided so to stay clear from very large while loops. Again, using $\epsilon = 0.01$ was a reasonable choice, which should once more imply, in average, around one collision per integration loop in each of the coordinates.

Gelman-Rudin coefficient was found to be of $\hat{R} = 1.05$ for 100 parallel chains, each of 1000 sampled points and with the same configurations of mass, $R$, $L$ and $\epsilon$ as before. This value is below the literature's suggested of $\hat{R} = 1.1$, reaffirming convergence of RHMC. Geweke diagnostic was also performed for 500 chains and histogram plot (Figure 5) indicates convergence of the difference between final and initial average of the chains to the desired (unormalized) Gaussian.

Figure 4 also shows that convergence of RHMC estimation seems much faster than exponential, suggesting (but does not guarantee) geometric ergocity. Figure 6 shows the estimated autocorrelation (11) for 100 chains of 1000 entries each and suggests that we might take the convergence of the series in the definition of effective sample size (10) to converge. Estimating $\tau^2$ from equation (8) through (12), where we take $k = 20$ after [Gamerman and Lopes (2006)], gives $\hat{\tau} = 1.20$ for $10^5$ samples, yielding a 95% interval based on the Central Limit Theorem in equation (13) of $[0.900, 0.913]$.

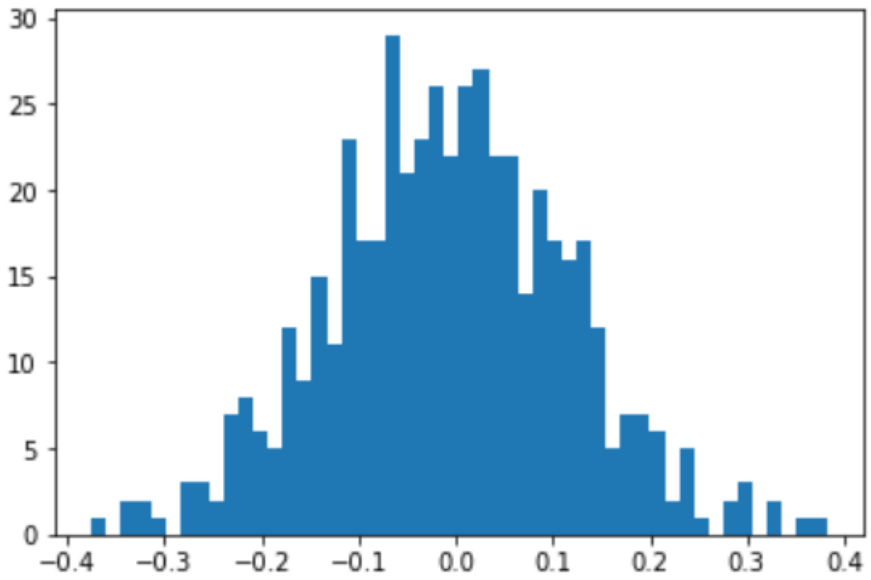


Figure 5: Histogram for the average distance of means of first 100 values and last 500 values of 500 RHMC chains, each of 1000 points, with all $m$ equal 1, $L = 100$, $\epsilon = 0.01$, and choosing $\mathbf{x}_0$ through a rejection sampling using an independent multidimensional normal distribution in $D$.

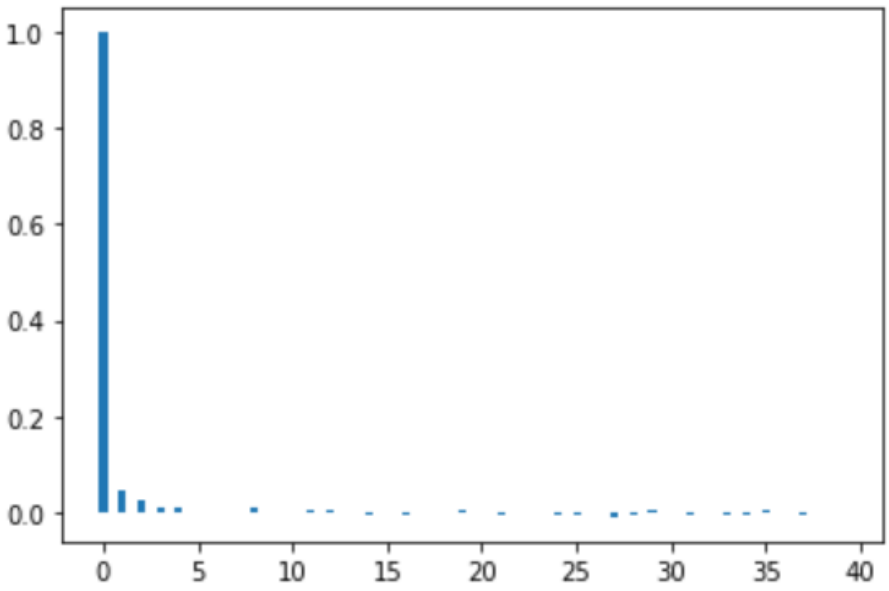


Figure 6: Autocorrelation plot for 100 RHMC chains of sizes 1000 each, with all $m$ equal 1, $L = 100$, $\epsilon = 0.01$, and choosing $\mathbf{x}_0$ through a rejection sampling using an independent multidimensional normal distribution in $D$..

Finally, we compute $\hat{I}_1$ for all $R$ values in $\{0.01, 0.1, 1, 10, 100, 1000, 10000\}$ with 500 chain runs for each $R$. Notice that the constraints on $\theta_1$ and $\theta_2$ are kept unchanged as we boost up the values of $R$, but the $r_1$ and $r_2$ stretch. To allow to keep the exploration of these new elongate spaces as efficient as for $R = 1$, it seems reasonable decreasing the variances of the momentum samplers $q(p_{r_1}|r_1)$ and $q(p_{r_2}|r_2)$, $m_{r_1}$ and $m_{r_2}$, since the average momentum magnitude follows $\sqrt{m}\sqrt{\frac{2}{\pi}}$ and the appropriate change in coordinate will be $\propto \frac{\|p\|}{m} = m^{-1/2}$. Consequently, we take $m = 1/R^2$.

Figure 7 shows a table of bias, variance, and the Monte Carlo Standard Error (MCSE) for each of these $R$ values. We take the MCSE defined by the square root of sample standard deviation of the chain, $\hat{\sigma} \approx \sqrt{\mathrm{Var}_\pi(\mathbf{x}_{(i)})}$, divided by the effective sample size $n_{eff}$, which by equation (10) gives

$$\mathrm{MCSE} = \sqrt{\frac{\hat{\sigma}^2}{n_{eff}}} = \sqrt{\frac{\hat{\sigma}^2}{n\hat{\sigma}^2/\hat{\tau}^2}} = \sqrt{\frac{\hat{\tau}^2}{n}},$$

allowing estimation through (12). Again, in estimating $\tau^2/n$, we kept $k = 20$, following [Gamerman and Lopes (2006)].

| | Bias | Variance | MCSE |
|---|---|---|---|
| **0.01** | -0.000007 | 1.315008e-04 | 0.000023 |
| **0.10** | 0.000074 | 1.312667e-02 | 0.000134 |
| **1.00** | 0.000868 | 1.315482e+00 | 0.001506 |
| **10.00** | 0.001769 | 1.317416e+02 | 0.021446 |
| **100.00** | -0.023654 | 1.314555e+04 | 0.169862 |
| **1000.00** | 0.978568 | 1.318585e+06 | 1.573698 |
| **10000.00** | -17.211298 | 1.308331e+08 | 16.186384 |

Figure 7: Table with bias, variance and Monte Carlo Standard Error (MCSE) of the estimator $\hat{I}_1$ with $\pi \sim U\_C$, sampled through RHMC for $R$ values in $\{0.01, 0.1, 1, 10, 100, 1000, 10000\}$, where the indices indicate $R$. We used a total of 500 chains with 1000 samples with $\epsilon = 0.01$, $L = 100$, $m_{\theta_1} = m_{\theta_2} = 1$, and $m_{r_1} = m_{r_2} = 1/R^2$.

# The General Solution to Boundary Complications [3, 4]

Sadly, RHMC we have developed thus far only works for affine constraints support, which is far from being the case for the target distribution $\pi_2$ used in $\hat{I}_2$, which is uniform in the circle $C_R \subseteq \mathbb{R}^2$. Thankfully, though, a generalization of the technique can be developed using the same Newtonian way-of-thinking.

Consider now a particle of mass $m$ in a $d$-dimensional space under the influence of a potential field $U(\mathbf{x})$ and with a momentum vector $\mathbf{p}$. This particle hits a boundary defined though some constraint equation of the coordinates $\mathbf{x}$, $G(\mathbf{x}) \leq 0$, enough differentiable so that $\nabla G$ exists. We may, thanks to Gram-Schmidt, decompose $\mathbf{p}$ into a component $\mathbf{p}_{\nabla G}$ parallel to $\nabla G$ and a set of $d-1$-components that span a hyperplane normal to it, which we shall denote by $\{\mathbf{p}^T_{\nabla G}\}$ (Figure 8). Then, since all the force of collision happens in the direction parallel to the gradient, as any other direction perpendicular to $\mathbf{p}_{\nabla G}$ allows (locally) for motion without any interaction with the boundary, the vectorial aspect of Newton's Second Law dictates that only $\mathbf{p}_{\nabla G}$ is allowed to changed, keeping $\mathbf{p}^T_{\nabla G}$ constant[7]. Since, by conservation of the Hamiltonian, $\|\mathbf{p}\|^2 = \|\mathbf{p}_{\nabla G}\|^2 + \|\mathbf{p}^T_{\nabla G}\|^2$ does not change because of the impact with the boundary, we have that, after the moment of contact,

$$\mathbf{p}_{\nabla G} = -\mathbf{p}_{\nabla G} \quad \mathbf{p}^T_{\nabla G} = \mathbf{p}^T_{\nabla G}.$$

Therefore, if we can find the projections $p_{\nabla G} = \langle \mathbf{p}, \hat{\nabla G} \rangle$ and $p^T_{\nabla G} = \langle \mathbf{p}, \hat{\nabla G}^T \rangle$, reverse $p_{\nabla G}$ to $p'_{\nabla G} = -p_{\nabla G}$ and project back to the original coordinate system,

[7] We drop the set notation in $\mathbf{p}^T_{\nabla G}$ from here on, but keep in mind that this corresponds to $d-1$ orthonormal vectors. Happily, things further simplify in the particular case of a 2-dimensional configuration space, since $\mathbf{p}^T_{\nabla G}$ will correspond to exactly one vector.

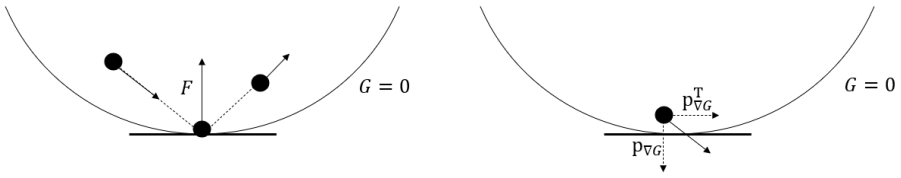


Figure 8: Diagrams showing a particle of mass $m$ and momentum $\mathbf{p}$ in a 2-dimensional configuration space approaching the boundary of some differential convex constraint $G(\mathbf{x}) \leq 0$. We notice that all the force that reflects the particle motion is restricted to the axis parallel to $\nabla G$, with no components in the perpendicular hyperplane, here indicated by the horizontal black line.

generating a new momentum $\mathbf{p}'$, we may use the same rationale in developing Algorithm 2 here as well. If we assume the support of the target distribution to be convex [8], and let $\mathbf{x}_0$ the point of impact, where the particle crosses to the forbidden region and $\Delta$ the amount of time the particle travels in this region, we have $\Delta = (\mathbf{x} - \mathbf{x}_0)\frac{p}{m}$. Therefore, being $(\mathbf{x}_{(i-1)}, \mathbf{p}_{(i-1)})$ the coordinates of the particle at the beginning of the time step in which the collision happens, $\mathbf{p}'$ the momentum right after the collision, the new proposal becomes

$$\mathbf{x}_{(i)} = \mathbf{x}_0 + \Delta\frac{\mathbf{p}'}{m} \quad \mathbf{p}_{(i)} = \mathbf{p}' - \Delta \cdot \nabla U|_{\mathbf{x}_0}.$$

For our particular case of sampling on $\pi_2 \sim U_{C_R}$, $U = \nabla U = 0$, $G(x, y) = x^2 + y^2 - R^2 \leq 0$, we see that $\nabla G = 2(x, y)$, which is normalized to $\nabla G = \frac{\mathbf{r}}{\|r\|} = \hat{\mathbf{r}}$, where $\hat{\mathbf{r}}$ is the unit vector in the radial direction. Working with polar coordinates makes things much easier in this scenario because the transforms from Cartesian to polar and back are widely known:

$$\begin{aligned} x = r\cos\theta \quad & y = r\sin\theta \\ r = \sqrt{x^2 + y^2} \quad & \theta = \arctan\frac{y}{x} \\ \hat{\mathbf{r}} = \cos\theta\,\hat{\mathbf{x}} + \sin\theta\,\hat{\mathbf{y}} \quad & \hat{\boldsymbol{\theta}} = -\sin\theta\,\hat{\mathbf{x}} + \cos\theta\,\hat{\mathbf{y}}. \end{aligned}$$

Letting $\dot{x} = p_x/m$ and $\dot{y} = p_y/m$ be the velocity components in $x$ and $y$ coordinates, we have that, differentiating the above with respect to time

$$\begin{aligned} \dot{x} = \dot{r}\cos\theta - r\dot{\theta}\sin\theta \quad & \dot{y} = \dot{r}\sin\theta + r\dot{\theta}\cos\theta \\ \dot{r} = \frac{\dot{x}x + \dot{y}y}{\sqrt{x^2 + y^2}} \quad & \dot{\theta} = \frac{-\dot{x}y + \dot{y}x}{x^2 + y^2}. \end{aligned}$$

Also differentiating by $\theta$ gives, $\frac{d\mathbf{r}}{d\theta} = \hat{\boldsymbol{\theta}}$ and $\frac{d\hat{\boldsymbol{\theta}}}{d\theta} = -\hat{\mathbf{r}}$, so

$$\dot{\mathbf{r}} = \frac{d}{dt}r\hat{\mathbf{r}} = \dot{r}\,\hat{\mathbf{r}} + r\frac{d\hat{\boldsymbol{\theta}}}{dt} = \dot{r}\,\hat{\mathbf{r}} + r\frac{d\hat{\boldsymbol{\theta}}}{d\theta}\dot{\theta} = \dot{r}\,\hat{\mathbf{r}} + r\dot{\theta}\,\hat{\boldsymbol{\theta}},$$

[8] Convexity is crucial here as it guarantees that if the particle leaves the support, it cannot alone return during an integration step time.

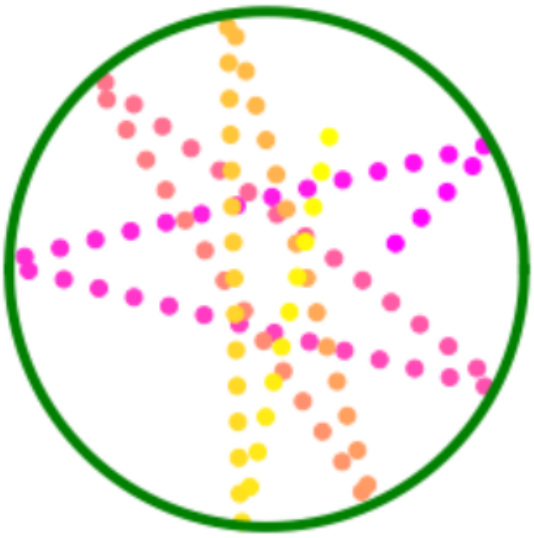

Figure 9: Each point represents a position at the end of a step of a single integration loop of Algorithm 3, suggest the billiard motion. Parameters were set for $R = 1$, $\epsilon = 0.1$ and $L = 100$. The dark green circle shows the boundary of the support of the target distribution $\pi_2 \sim U_{C_R}$, i.e. a circle of radius $R$.

by consecutive applications of the product and chain rules.

If we allow for the momentum just *prior to* the collision (where $r = R$) to be

$$\mathbf{p} = m\dot{\mathbf{r}} = m\dot{r}\,\hat{\mathbf{r}} + mR\dot{\theta}\,\hat{\boldsymbol{\theta}} = m\dot{x}\,\hat{\mathbf{x}} + m\dot{y}\,\hat{\mathbf{y}},$$

we have that the momentum $\mathbf{p}'$ right *after* the collision is found by negating $p_r$ and keeping $p_\theta$ unchanged, that is

$$p'_r = -p_r = -m\dot{r} \quad p'_\theta = mR\dot{\theta},$$

which substituting into the momentum components for $x$ and $y$ gives

$$p'_x = p'_r\cos\theta - p'_\theta\sin\theta \quad p'_y = p'_r\sin\theta + p'_\theta\cos\theta.$$

Finally, we note theta $\Delta = m\frac{r-R}{\dot{r}}$, where $r = \sqrt{x^2+y^2}$ is the point where the particle would reach at the end of the integration step if no reflection took place at the boundary.

The full process of a single time step leapfrog update for the generalized RHMC in our particular case is summarized in Algorithm 3. Again, it is necessary to show that the resulting chain is reversible, has the canonical distribution as stationary and preserves volumes, since [Afshar et al. (2015)] only demonstrates these for the affine boundary case. The first two of these assertions follow from the same rationale in the affine scenario, but the symplectic property of the new integrator requires more effort and we found no work in literature either proving or contradicting this result. Nonetheless, our specific situation enjoys the very nice simplifications introduced by polar coordinates: if $\Phi_\epsilon$ is the map which takes the initial state at the beginning of the time step $(\mathbf{x}_{(i-1)}, \mathbf{p}_{(i-1)})$

to $(\mathbf{x}_{(i)}, \mathbf{p}_{(i)})$ through generalized RHMC leapfrog, we must only show that the associated Jacobian determinant, denoted $|\Phi_\epsilon|$, is one. If we perform the full analysis in a polar system, letting $J$ the bijective map from Cartesian coordinates to polar, then

$$J^{-1} \circ \Phi_\epsilon^{polar} \circ J = \Phi_\epsilon,$$

where $\Phi_\epsilon^{polar}$ is the map in polar coordinates of the leapfrog step. However, in polar, the constraints become

$$0 \leq r \leq R \quad \theta \text{ free but periodic,}$$

reducing, therefore, to the affine case where an argument of volume preservation already exists, i.e. $|\Phi_\epsilon^{polar}| = 1$. As $|\Phi_\epsilon| = |J^{-1}||\Phi_\epsilon^{polar}||J|$ and $|J^{-1}||J| = 1$, it follows that $|\Phi_\epsilon| = 1$, completing the proof that Algorithm 3 is symplectic.

**Algorithm 3** Single Leapfrog Time Step in Generalized RHMC for sampling $\pi \sim U_{C_R}$

Suppose we are within some integration period of size $\epsilon L$ and $(\mathbf{x}_{(i-1)}, \mathbf{p}_{(i-1)}$ are the coordinates at the beginning of the time step
$p_j \leftarrow p_j$ ▷ Just a formality because $\nabla U = 0$
$x_j \leftarrow x_j + \epsilon \frac{p_j}{m_j}$
**while** $x^2 + y^2 > R^2$ **do**:
$\theta = \arctan \frac{y}{x}$ ▷ Care must be taken for the arctan to fall within the correct quadrant
$\dot{r} \leftarrow frac\dot{x}x + \dot{y}y\sqrt{x^2 + y^2}$
$\dot{\theta} \leftarrow \frac{-\dot{x}y + \dot{y}x}{x^2+y^2}$
$\dot{r} \leftarrow -\dot{r}$ ▷ Equivalent to negating $p_r$
$\Delta \leftarrow m\frac{r-R}{\dot{r}}$
$p_x \leftarrow m\dot{r}\cos\theta - mR\dot{\theta}\sin\theta$
$p_y \leftarrow m\dot{r}\sin\theta + mR\dot{\theta}\cos\theta$
$x \leftarrow R\cos\theta + \Delta\frac{p_x}{m}$ ▷ Because the point of impact has $x = R\cos\theta$
$y \leftarrow R\sin\theta + \Delta\frac{p_y}{m}$ ▷ Because the point of impact has $y = R\sin\theta$
**end while**
$p_j \leftarrow p_j$ ▷ Again just a formality because $\nabla U = 0$

We are now in position to use generalized RHMC to sample from $\pi_2 \sim U_{C_R}$. Figure 9 shows a single integration time iteration of Algorithm 3 for $R = 1$, $m = 1$, $\epsilon = 0.1$, $L = 100$. Notice the visual aspect that resembles exactly what one would expect from a free particle ($U = 0$) surrounded by a circular infinite well: motion which literature calls *billiard*. Once more, to sample $\pi_2$ from the method above, it seems reasonable to use values of $\epsilon$ and $L$ that allow for, in average, one reflection per integration time. Since $p_r$, has, statistically speaking, same order of magnitude of $p_x$ and $p_y$ and the space we are sampling has radial size $R$, it is again suitable to let, for $m = 1$, $\epsilon \approx 0.01$. Empirically, it turned out that such a choice of $\epsilon$ led to 0.80 collisions with the boundary per integration loop.

This time around, however, restricting the number of boundary reflections is not only a computational choice important for decreasing the running time of while loops, but it also seems to impact the effectiveness of the sampler in reproducing $\pi_2$. Figure 10 shows 2-dimensional histograms of 10000 points

with increasing values of $\epsilon$. For $\epsilon$ small, as it is the case of $\epsilon = 0.001$, the sampler does not have time to fully explore the space, so the result is very concentrated in a certain region (specifically, in the second quadrant, but that depends on the particular values of initial positions $x_{(0)}$ and $y_{(0)}$). For $\epsilon = 0.01$, the empirical distribution seems a pretty accurate sampling of $\pi_2 \sim U_{C_R}$, again suggesting that maintaining around one reflection per integration loop is appropriate. However, the bigger $\epsilon$ becomes, the more apparent a centrality tendency of the sampled points shows up, tendency that does *not* exist for the target $\pi_2 \sim U_{C_R}$. Therefore, it seems that the many collisions produce some "pressure" in the the sampling process, forcing the points towards $R = 0$. We were unable to detect this kind of pressure for the affine boundary case even for larger choices of $\epsilon$, suggesting that it probably has to do with the geometry of the support of $\pi_2$ [9].

We can easily quantify whether the generated distribution has this centrality feature or not: calculate the ratio of points whose radius is smaller than $\frac{1}{\sqrt{2}}R$ over the total number of samples. Since for any uniform distribution, the probability of finding a point in a region of area $A$ is the ratio of $A$ and the total area of the support, it follows that if Algorithm 3 does a good job in sampling $\pi_2 \sim U_{C_R}$,

$$\hat{P} = \frac{\#\text{ points of radius less than } \frac{1}{\sqrt{2}}}{\#\text{ total sampled points}} = \frac{(R/\sqrt{2})^2\pi}{R^2\pi} = \frac{1}{2}.$$

Consequently, values much superior to $1/2$ for the quantity above indicate centrality tendencies. For $\epsilon = 0.01$, this $\hat{P}$ was equal to 0.5, but $\epsilon = 0.1$ and $\epsilon = 1$ yield, respectively, to $\hat{P} = 0.65$ and $\hat{P} = 0.72$, suggesting that the radial pressure which we identified in the histograms of Figure 10 can also be numerially measured. Therefore, from here on, we will only use $\epsilon = 0.01$, leaving the task of explaining this "centrality pressure" to future works. Nonetheless, it is noteworthy that [Gryazina and Polyak (2014)] circumvents this issue by taking two measures: 1. restricting the maximum number of reflections in every integration time, halting the algorithm if the collisions with the boundary are over such a value; 2. stochastically choosing the integration time $L$ at every loop. With such assumptions (specially the first one), the authors were able to prove convergence of their algorithm (very similar to Algorithm 3) to uniform distributions on any compact convex support, but they do not even mention the existence of what I called centrality pressure when 1 and 2 are not taken into consideration.

Finally, we may use the generalized RHMC to compute $\hat{I}_2$ given through (3). The top row of Figure 11 shows trace plots created from the application of Algorithm 3 for increasing number of sampled points (left) and number of 1000 samples chains (right), with a 30-iteration warm-up period, together with the theoretically predicted value (red) of $\frac{128}{45\pi}$. We have set $m = 1$, $L = 100$, $R = 1$ and chose $(x_{(0)}, y_{(0)})$ through rejection sampling of an independent mixed bivariate normal standard normal distribution. Once more, not only there seems to be convergence towards the result of equation (1), but this convergence seems

[9] At first, I thought the reason for this centrality pressure was related to the curvature of the boundaries, which for the affine case is 0, but for the disk interior is of $1/R$. However, by increasing $R$ and decreasing $m$, the same sort of phenomena took place: values of $\epsilon > 0.1$ resulted in awful samples of $\pi_2 \sim U_{C_R}$.

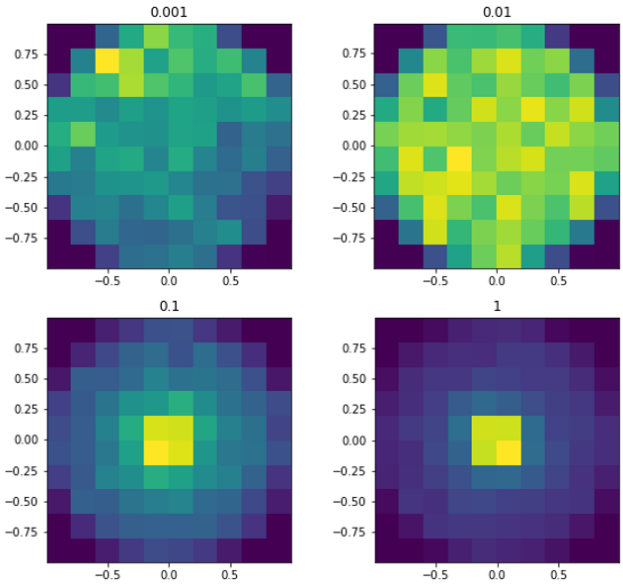


Figure 10: Two-dimensional histograms showing the distributions obtained through sampling 10000 using Algorithm 3 with $\epsilon = 0.001, 0.01, 0.1$, and 1. The bluer the region, the less populated it is. We used $R = 1$, $m = 1$ and $L = 100$.

fast; in fact even faster than the convergence of $\hat{I}_1$. The bottom left plot in Figure 11 shows Geweke diagnostic for $\hat{I}_2$, which also resembles a Gaussian, once more suggesting efficiency of the estimator. Additionally, we found Gelman-Rudin's $\hat{R}$ of $\hat{I}_2$ to be $\hat{R} = 1.05$, for 100 chains with 1000 sampled points each.

The bottom right plot of Figure 11 displays the autocorrelation factors of 100 chains of 1000 points each of the generalized RHMC. Once more, the decay is mostly likely smaller than $1/k^2$, which makes estimation of $\hat{\tau}^2$ potentially meaningful. We found $\hat{\tau}^2$ to be 0.11 for $10^5$, which, provided geometric ergocity, gives a 95% condifence interval of $[0.903, 0.908]$.

To conclude, Figure 12 gives a table of bias, variance and MCSE for 500 chains of 1000 samples long and $R \in \{0.01, 0.1, 1, 10, 100, 1000, 10000\}$. We used the same technique of setting $m = \frac{1}{R^2}$ to account for increasing scale, keeping $\epsilon$ and $L$ constant at 0.01 and 100, respectively.

## Comparing Approaches [5]

Contrasting the standard RHMC sampler in calculating $\hat{I}_1$ and the generalized version in calculating $\hat{I}_2$ through Figures 7 and 12, it is clear that $\hat{I}_2$ outperforms $\hat{I}_1$ in variance(s), specially for larger $R$, but the biases of both methods seem fairly comparable. Besides, $\hat{I}_2$ comes with an additional simplification in interpretability, since it is constructed directly from the original problem of calculating distances from uniform distributions in the disk, $\pi_2 \sim U_{C_R}$, without appealing at all to writing complicated integral forms, such as equation (1).

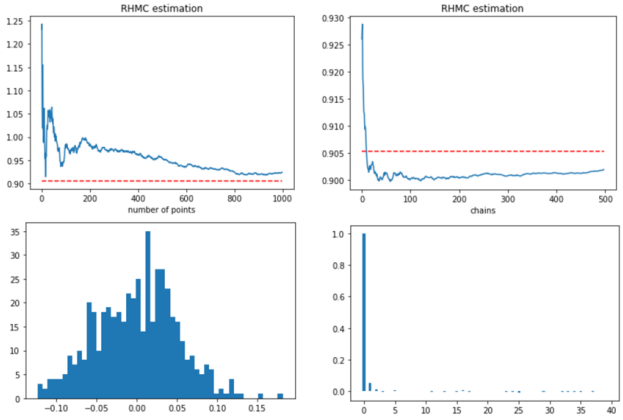


Figure 11: Some plots regarding the convergence of $\hat{I}_2$ with $\pi_2 \sim U_{C_R}$ sampled with Algorithm 3 (generalized RHMC). The top row shows traceplots for increasing number of sampled points (left) and increasing number of 1000-sample long chains (right) with $\epsilon = 0.01$, $L = 100$, $R = 1$, and $m = 1$. The red dashed line in both of these figures indicates the theoretical value of convergence of $\hat{I}_2 = \frac{128}{45\pi}$. The bottom left figure exhibits a Geweke diagram for the process, which, thanks to its Gaussian-like shape, is a sign of good convergence. The bottom right plot shows the autocorrelation factors estimated through equation (11) for lags ranging from $k = 0$ to $k = 40$.

This allows for some pretty meaningful diagnostics such as histograms and $\hat{P}$ to access the efficiency of the general RHMC in sampling $\pi_2$. Of course, there are equivalent tests for affine boundary RHMC sampler used in estimating $\hat{I}_1$, such as displaying the histograms for each of the directions $r_1, r_2, \theta_1$ and $\theta_2$, as well as quantitative analysis similar to $\hat{P}$, but these tests are, perhaps, not as intuitive as the correspondent ones for the generalized RHMC.

Nonetheless, all these benefits come with a cost and, in this case the cost is computational[10]. While the standard RHMC took only 307 seconds in my machine to compute the table in Figure 7, the generalized RHMC took 4024 seconds to compute Figure 12. Therefore, even though we were able to recover better results using the generalized method, the increase in computational effort barely justifies the use the generalized RHMC to solve this particular situation instead of the more traditional technique (although the reader must agree that the second approach is, by far, more elegant). Neither of these numbers, however, do not look so big when compared to the time estimated to compute the same number of samples with very simple rejection sampler I used in Assignment 0 to estimate $\hat{I}_2$: 126 days.

Before I close off, I would like to mention some other techniques that related to HMC and may be used in solving this particular problem, which I was not able to explore due to time constraints. First, I do not believe that the most common of these modified methods, the no U-turn, would bring much improvements as its main goal is to keep acceptance rate high, value which is

[10]This, hopefully, answers question 5, that is, the computational effort is a key quantity to take into account in the choice of most suitable sampling technique for a given problem.

| | Bias | Variance | MCSE |
|---|---|---|---|
| **0.01** | -0.000024 | 1.786967e-05 | 0.000007 |
| **0.10** | -0.000346 | 1.795330e-03 | 0.000057 |
| **1.00** | -0.003777 | 1.788460e-01 | 0.000745 |
| **10.00** | -0.031566 | 1.791573e+01 | 0.006004 |
| **100.00** | -0.281657 | 1.791213e+03 | 0.065428 |
| **1000.00** | -2.987958 | 1.789864e+05 | 0.468458 |
| **10000.00** | -39.747440 | 1.791100e+07 | 6.188455 |

Figure 12: Table with bias, variance and Monte Carlo Standard Error (MCSE) of the estimator $\hat{I}_2$ with $\pi \sim U_C$, sampled through generalized RHMC for $R$ values in $\{0.01, 0.1, 1, 10, 100, 1000, 10000\}$, where the indices indicate $R$. We used a total of 500 chains with 1000 samples with $\epsilon = 0.01$, $L = 100$, $m = 1/R^2$.

already at 100% for both samplers. A more interesting suggestion, however, is offered by [Mohasel Afshar et al. (2021)] which simplifies reflections in the case of non-affine boundaries, unfortunately at the cost of relaxing the volume preservation assumption of integration. This method is called FORMAL by the authors and, even though they claim it to perform slightly worse than the generalized RHMC for simple non-affine boundary supports (such as the support of $\pi_2$), it can more easily be extrapolated to situations in which the simplifications introduced by different coordinate systems, as the polar approach we took, is not possible. Finally, [Girolami and Calderhead (2011)] famous paper introduces techniques that extend HMC to manifolds other than flat Cartesian, thus allowing the development of algorithmic techniques to sample uniformly at the disk $C_R$ with references to polar coordinates only, possibly simplifying Algorithm 3. Nonetheless, this extra freedom in coordinates requires appropriate changes in the kinetic energy term $T$, making the proposal distribution $q(\mathbf{p}|\mathbf{x})$ potentially more complicated.

# Bibliography


Afshar, H. M., Domke, J., et al. (2015). Reflection, refraction, and hamiltonian monte carlo. In *NIPS*, pages 3007–3015.

Beck, M. (2012). *Quantum mechanics theory and experiment*. Oxford University Press.

Betancourt, M. (2018). A conceptual introduction to hamiltonian monte carlo.

Chevallier, A., Pion, S., and Cazals, F. (2018). *Hamiltonian Monte Carlo with boundary reflections, and application to polytope volume calculations*. PhD thesis, INRIA Sophia Antipolis, France.

Gamerman, D. and Lopes, H. F. (2006). *Markov chain Monte Carlo: stochastic simulation for Bayesian inference*. Taylor & Francis.

Gelman, A. and Rubin, D. B. (1992). A single series from the gibbs sampler provides a false sense of security. *Bayesian statistics*, 4:625–631.

Geweke, J. F. (1991). Evaluating the accuracy of sampling-based approaches to the calculation of posterior moments. Staff Report 148, Federal Reserve Bank of Minneapolis.

Girolami, M. and Calderhead, B. (2011). Riemann manifold langevin and hamiltonian monte carlo methods. *Journal of the Royal Statistical Society: Series B (Statistical Methodology)*, 73(2):123–214.

Gryazina, E. and Polyak, B. (2014). Random sampling: Billiard walk algorithm. *European Journal of Operational Research*, 238(2):497–504.

Harris, R. (2016). *Modern physics*. Pearson India Education Services Pvt. Ltd.

Liouville, J. (1838). Note sur la théorie de la variation des constantes arbitraires. *Journal de Mathématiques Pures et Appliquées*, pages 342–349.

Livingstone, S., Betancourt, M., Byrne, S., and Girolami, M. (2019). On the geometric ergodicity of Hamiltonian Monte Carlo. *Bernoulli*, 25(4A):3109 – 3138.

Mohasel Afshar, H., Oliveira, R., and Cripps, S. (2021). Non-volume preserving hamiltonian monte carlo and no-u-turnsamplers. In Banerjee, A. and Fukumizu, K., editors, *Proceedings of The 24th International Conference on Artificial Intelligence and Statistics*, volume 130 of *Proceedings of Machine Learning Research*, pages 1675–1683. PMLR.

Neal, R. (2011). Mcmc using hamiltonian dynamics. *Chapman & Hall/CRC Handbooks of Modern Statistical Methods Handbook of Markov Chain Monte Carlo*.

Pakman, A. and Paninski, L. (2014). Exact hamiltonian monte carlo for truncated multivariate gaussians. *Journal of Computational and Graphical Statistics*, 23(2):518–542.

Ruján, P. (1997). Playing billiards in version space. *Neural Computation*, 9(1):99–122.

Singer, I. M. and Thorpe, J. A. (2012). *Lecture notes on elementary topology and geometry*. Springer-Verlag.

Taylor, J. R. (2005). *Classical mechanics*. University Science Books.